Microfluidically Synthesized Au, Pd and AuPd Nanoparticles Supported on SnO_2 for Gas Sensing Applications

Ghazal Tofighi[a,1], David Degler[b,1,2], Benjamin Junker[b], Sabrina Müller[a], Henning Lichtenberg[a,c], Wu Wang[d], Udo Weimar[b], Nicolae Barsan[b,], and Jan-Dierk Grunwaldt[a,c,*]*

[a] Institute for Chemical Technology and Polymer Chemistry (ITCP), Karlsruhe Institute of Technology (KIT), Engesserstr. 20, D-76131 Karlsruhe, Germany

[b] Institute of Physical and Theoretical Chemistry and Centre for Light-Matter Interaction, Sensors & Analytics (LISA+), University of Tübingen, D-72076 Tübingen, Germany

[c] Institute of Catalysis Research and Technology (IKFT), Karlsruhe Institute of Technology (KIT), D-76344 Eggenstein-Leopoldshafen, Germany

[d] Institute of Nanotechnology (INT), Karlsruhe Institute of Technology (KIT), D-76344 Eggenstein-Leopoldshafen, Germany

* Corresponding authors: nb@ipc.uni-tuebingen.de; grunwaldt@kit.edu

Tel.: +49 721 608-42120

Fax: +49 721 608-44820

[1] Ghazal Tofighi and David Degler contributed equally to this work.

[2] Present address: European Synchrotron Radiation Facility (ESRF), F-38043 Grenoble, France.

Abstract

Monometallic Au and Pd nanoparticles (NPs) and homogeneous AuPd nanoalloy particles were synthesized in a continuous flow of reactants ($HAuCl_4$, K_2PdCl_4, $NaBH_4$ and polyvinylpyrrolidone (PVP)) using a microfluidic reactor with efficient micromixers. The obtained ultrasmall NPs were subsequently deposited onto SnO_2 supports with different surface area (32.7 and 3.6 m^2 g^{-1}). Samples with 1.0 and 0.1 wt.% metal loading were prepared. After calcination at 380 °C for 1 h the supported NPs aggregated to some extent. SnO_2 supported AuPd nanoalloys with low (0.1 wt.%) metal loadings showed the smallest NP diameters (~ 5 - 7 nm) and the narrowest size distribution among the samples. The gas sensing performance of the materials was investigated at 300 °C in four different gas atmospheres containing either CO, CH_4, ethanol or toluene using dry and humid conditions. They exhibited a distinct variation in the response patterns and selectivity toward the test gases depending on composition and metal loading: Au increased the sensor signals compared to pristine SnO_2 in all cases and decreased the interference of water vapor; the supported Pd NPs showed a weak response to toluene, strong sensitivity in CO sensing and slightly better response in ethanol sensing in humid air compared to dry air. However, they showed a high selectivity toward CH_4 when used in dry air; AuPd alloy particles provided lower sensor signals compared to pristine SnO_2 and no remarkable CH_4 selectivity, in contrast to the Pd system. Operando diffuse reflectance infrared Fourier-transformed spectroscopy (DRIFTS) indicates a strong band bending in the case of Pd and AuPd NPs, whereas in the case of Au no band bending occured, indicating a strong electronic interaction between the support and Pd-containing NPs (Fermi-level control mechanism), and a weak electronic interaction between SnO_2 and Au NPs (spill-over mechanism).

Keywords: Microfluidic synthesis, AuPd nanoalloy, Gold, Palladium, SnO_2, Gas sensor

1. Introduction

Gas sensing has become increasingly important in our society due to technical innovations and the higher living standard[1-4]. Semiconducting metal oxide (SMOX) based materials are widely applied in the field of gas sensing for safety, quality control and personnel protection. Their applications range from gas bottle leak detection[5] to air quality monitoring, e.g. air intake in cars[1, 6].

Most SMOX sensors are based on SnO_2 which has proven to be one of the most inexpensive, best performing and most stable sensing materials for reducing gases[7, 8]. The gas sensing mechanism in pristine SMOX is based on the reception of gases, i.e. a surface reaction changing the free charge carrier concentration at the surface, and transduction, which translates the changes in the charge carrier concentration into an electronic signal[1]. A detailed discussion of the fundamental gas sensing mechanism of SMOX is found elsewhere[9-11].

Pristine SMOX have excellent gas sensing properties in dry air, but lack selectivity and long-term stability[11], and show a strong cross-interference of water vapor[9]. A solution to overcome these issues is the introduction of noble or transition metals in low concentration (0.1-2.0 wt%) into the sensing materials[12-15]. Additives can be present as dispersed nanoparticles (NPs), oxidized clusters, i.e. loadings, or as ions incorporated into the SnO_2 lattice, i.e. dopants. Depending on their chemical state, distribution and dispersion, the metal NPs either influence the reception (chemical properties) and/or transduction (electronic properties) of the base material[11, 16]. When metallic NPs are present at the surface of the sensing materials, they are assumed to affect the chemical reaction of the target gas or gaseous reaction partners by activation of the gases at the NP surface and/or their subsequent spill-over to the SnO_2 surface (spill-over mechanism). If the metals are present as oxidized clusters, they are in close contact with the SMOX, affecting the chemical and

electronic properties of the SnO_2, e.g. the Fermi-level of SnO_2 (Fermi-level control mechanism)[17-20].

A very good example for a dopant leading to spill-over in CO sensing is Au[21-23]. Generally, the Au loadings are found in metallic state on the surface of the SnO_2 sensing material and do not change the surface or bulk electronic properties of the SnO_2[13, 16, 21, 22, 24]. In previous works, an oxygen-related spill-over sensitization was found for Au NPs on SnO_2[22,23]. Combined work function and resistance measurements show no electronic interaction of Au and SnO_2[22] and High Energy Resolution Fluorescence Detection X-ray Absorption Spectroscopy (HERFD-XAS) and Diffuse Reflectance Infrared Fourier-Transformed Spectroscopy (DRIFTS) indicate additional oxygen species on the surface of Au-loaded SnO_2[25].

The second generally accepted sensitization mechanism is the Fermi-level control mechanism, which is expected for oxidized metal loading like in the case of Pt[19, 26] or Pd[27, 28] supported on SnO_2. If deposited onto SnO_2, Pd is present as clusters. Due to the close contact of the oxidized Pd with the SnO_2 base material an electronic coupling between the oxidized Pd and SnO_2 occurs. The strength of this coupling is determined by the stoichiometry of the noble metal loading, i.e. PdO. If PdO is partially reduced, the electronic coupling is altered and directly affects the charge transport in SnO_2 (transduction) and therefore the sensors' output signal[29].

With the knowledge that sensing materials loaded with monometallic Au or Pd as dopants lead to spill-over and the Fermi-level control sensing mechanism, respectively, it is intriguing to examine the effect of the two metals being combined as an alloy. Recently, Tofighi et al.[30, 31] introduced an innovative method to produce monodisperse mono- and homogeneously mixed bimetallic nanocolloids in aqueous suspension in a one-step microfluidic synthesis process. The obtained NPs can be subsequently deposited onto metal oxide supports, i.e. materials attractive for catalysis

and gas sensing. The aim of this study is to trigger the sensing properties, e.g. selectivity, by preparing noble metal NPs including well-mixed AuPd nanoalloys using a microfluidic reactor, to study their response with respect to various reducing gases and the dominant mechanism involved.

2. Materials and methods

2.1. Materials

$HAuCl_4 \cdot 3H_2O$ (Roth, 99.5% purity), K_2PdCl_4 (Alfa Aesar, 99.99% purity), polyvinylpyrrolidone (PVP, Sigma-Aldrich, average molecular weight 40 kDa), $NaBH_4$ (Sigma-Aldrich, 99.99% purity), H_2SO_4 (Sigma-Aldrich, 95% solution) were used without purification. $SnCl_4$ purchased from Merck was purified by distillation.

2.2. Microfluidic synthesis of Au, Pd and AuPd nanoparticles

The colloidal route for synthesis of ultrasmall Au, Pd and AuPd NPs using a microfluidic reactor was adopted from our previous reports[30, 31] and Hayashi et. al[32]. An aqueous solution of metal precursors (7.5 mM) with 666 mg PVP was prepared for all samples with nominal molar Au:Pd ratios of 1:0, 1:1 and 0:1. $NaBH_4$ aqueous solution (37.5 mM) with 666 mg PVP was prepared as the reducing agent. These two solutions were poured separately into the corresponding vessels of the microfluidic setup (Fig. 1), which under 13 bar N_2 gas pressure generates a continuous and pulsation-free flow of reactants at high flow rates (2.6 L h^{-1} achieving 2400 Reynolds number). The pressurized reactants were injected into three cyclone micromixers for fast, efficient and homogeneous mixing in 2 ms (necessary for fast reduction reactions), and followed by a meandering microchannel for controlled nucleation and growth of NPs. Finally, the synthesized NPs were collected in a round-bottom flask placed in an ice/water bath and stirred for 1 h.

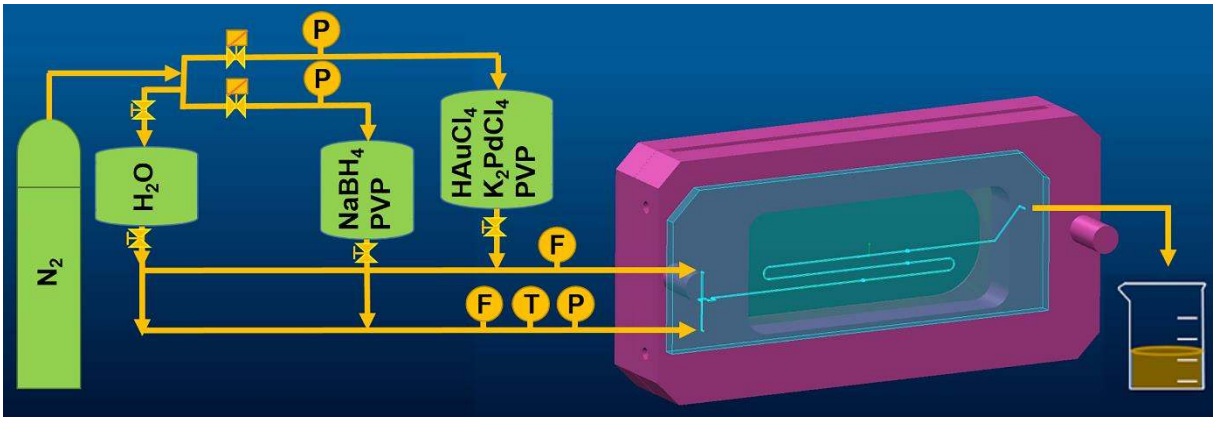

Fig. 1 Microfluidic apparatus for colloidal nanoparticle synthesis in continuous flow with reactant vessels and microfluidic chip (F, T and P: flowmeter, temperature sensor and pressure transducer). The microfluidic chip made of Si-glass bonded wafer is fixed in a stainless steel support frame.

2.3. SnO_2 synthesis

SnO_2 with two different surface areas were synthesized by an aqueous sol-gel method with $SnCl_4$ as precursor[33]. The precipitated solid material was separated by centrifugation, washed several times and dried at 120 °C. Afterwards, the product was divided into two samples, one calcined at 450 °C (SnO_2-450) and the other at 1000 °C (SnO_2-1000) for 8 h under air leading to surface areas of 32.7 and 3.6 $m^2\ g^{-1}$, respectively. Spectroscopic investigations by DRIFTS[34, 35] and UV/vis-DRS[36] and electronic studies of the conduction mechanisms[37, 38] for two base materials are reported elsewhere. The spectroscopic investigations reveal strong difference in the surface chemistry and optical band gap, while the electronic studies exhibit the same conduction mechanism for both materials, namely a depletion layer-controlled conduction involving grains with an unaffected bulk region.

2.4. Preparation of Au, Pd and AuPd nanoparticles supported on SnO_2

The metal NP solution produced in the microreactor was added to a suspension of 1 g SnO_2 in 80 mL water acidified with 10 mL H_2SO_4 solution (0.58 M) while stirring at room temperature for 1

h. After adsorption of the metal colloids on the support, the suspension was centrifuged three times (4500 rpm, 5 min each) and washed with water until pH 5-6 was achieved. Subsequently, the material was dried at 80 °C overnight. Afterwards, the samples were calcined at 380 °C for 1 h. This method was used to prepare sensor materials with 0.1 wt% and 1.0 wt% Au, Pd and AuPd supported on SnO_2-450 and SnO_2-1000, respectively.

2.5. Characterization of gas sensor materials

2.5.1. Gas sensor preparation and gas sensing measurements

Gas sensors were made by screen printing a paste, made from undoped or metal-doped SnO_2 powders and an organic binder (propanediol), on alumina substrates equipped with interdigitated Pt-electrodes and a backside heating meander (Pt)[39]. Gases were mixed using home-made gas dosing units with mass flow controllers, addition the diluted analyte gas to the carrier gas stream (synthetic air, 20.5 vol.% O_2) with a total flow of 250 sccm. Humidity levels were dosed by using evaporators filled with deionized water. All gases were supplied by Westfalen AG Münster. When measuring in N_2 atmospheres, the residual oxygen concentration in the gas flow was determined using a solid-state electrochemical oxygen sensor (Zirox SGM 400), which was placed downstream of the measured samples. The sensors were heated by applying a specific voltage and current to the backside heaters using a DC-powder supply (Agilent E3614A) and adjusting the exact values according to the sensor's temperature calibration. All experiments were conducted at 300 °C. The sensor response (resistance R) was measured using a digital multimeter (Agilent 34410A). All experiments were performed by measuring one sensor at a time to avoid downstream effects. For reducing gases the sensor signal was calculated as the ratio ($S = R_0 / R_{gas}$) of the baseline resistance (R_0) and the resistance during gas exposure (R_{gas}).

2.5.2. Electron microscopy

Electron microscopy was carried out using a scanning transmission electron microscope (STEM) with high angle annular dark-field detector (HAADF) and the composition of the samples was investigated by energy dispersive X-ray spectroscopy (EDX) using an EDAX S-UTW EDX detector in a FEI Titan 80-300 microscope operating at 300 kV. The gas sensor samples were directly dispersed on Cu grids coated with holey carbon film. Particle size statistics of the specimens were carried out on HAADF-STEM images by the ImageJ 1.49v software[40] assuming particles with ellipsoid shapes.

2.5.3. Diffuse reflectance FTIR spectroscopy

All FTIR spectra were recorded in diffuse reflectance geometry (DRIFTS) using a N_2-purged Bruker Equinox55 FT-IR spectrometer equipped with a six-mirror optic (Harrick Praying Mantis). The sensors were placed in a homemade operando cell[41], which was installed in the six-mirror optic. All single channel spectra were recorded with a resolution of 4 cm^{-1} and 1024 scans per spectrum. Absorbance spectra were calculated using Lambert-Beer's law, taking a single channel spectrum recorded in absence of CO, i.e. in dry or humid air, as reference[42]. Gas dosing, heating of sensors and electrical measurements were performed as described in 2.5.1.

3. Results and discussion

3.1. Gas sensing performances

The prepared gas sensors were tested at 300 °C in dry and humid air (50% r.h. at 25 °C) and the results are shown in Fig. 2-4 and Fig. S1. The gas sensing properties of the noble metal loaded SnO_2 samples differ from the corresponding pristine SnO_2 materials (shown in blue).

3.1.1. Au-loaded samples

In the case of SnO_2-1000, the presence of Au causes an enhancement of all sensor signals compared to the pristine material (Fig. 2a). By comparing the impact of water vapor on the sensing

properties of pristine and Au-loaded SnO_2-1000, different observations are made. In case of CH_4 and ethanol similar trends are observed for both materials, namely a decrease in CH_4 signals and a slight increase in the ethanol signals in humid air. The presence of Au NPs strongly decreases the influence of humidity on the CO signal, which now causes only a minor decrease in the CO signal in humid air. In case of toluene, Au-loading enhances the toluene signals in humid air instead of decreasing them, as observed for pristine SnO_2-1000. These observations are in line with the expectations for the sensitization effect of Au NPs: The activation of oxygen by Au NPs and subsequent spill-over increase the reactivity of the SnO_2 surface and thus enhances the gas reception on SnO_2 with minor effects on the selectivity[22, 23]. A similar pattern is found for Au NPs deposited on SnO_2-450 (Fig. 2b), but with two differences: Compared to pristine SnO_2 in dry air, the sensor signals for methane and toluene are respectively decreased by a factor of 1.8 and 2.5; probably due to the expected higher overall reactivity of the high-surface area SnO_2-450 with 1 wt.% Au loading. The effect of water vapor in the case of Au/SnO_2-450 and pristine SnO_2-450 is different quantitatively in the case of ethanol and qualitatively in the case of CO. The ethanol sensing signals of Au-/SnO_2-450 markedly increase, while for Au/SnO_2-1000 this increase is less pronounced. In the case of CO sensing, the presence of water vapor increases the signals of Au/SnO_2-450, while for Au/SnO_2-1000 a small decrease is observed. Since water vapor has different effects on the CO and EtOH sensing properties of both base materials (Fig. S2) and H_2O causes different chemical and electrical effects on both SnO_2 surfaces[34, 43], the observations on the Au-loaded materials can be explained by different properties of the SnO_2 surfaces. With respect to the responses to the four tested gases, the effect of Au NPs on both SnO_2 materials follows a similar pattern (Fig. 2a,b), slightly affected by the properties of the base materials.

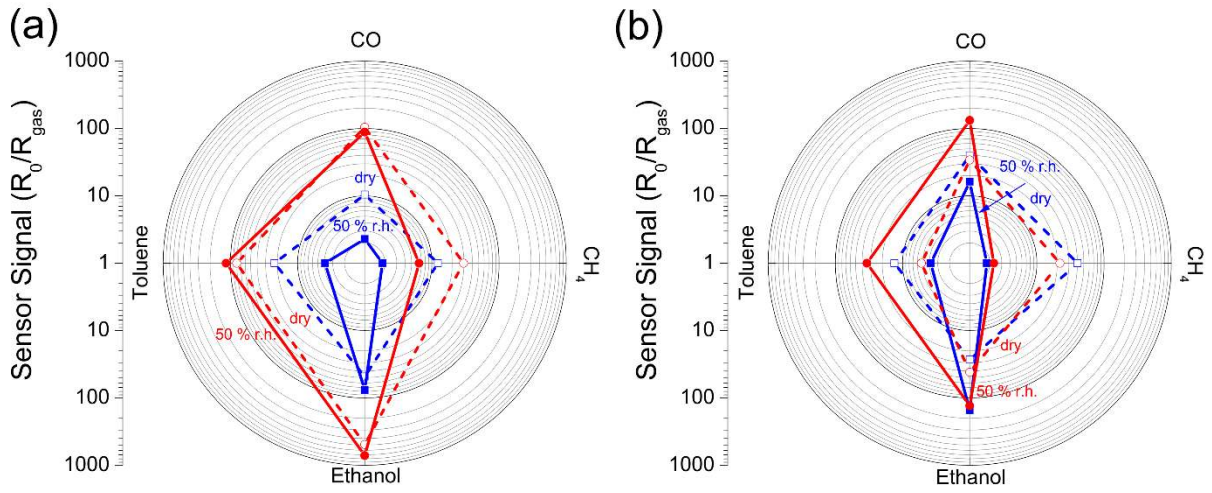

Fig. 2 Polar plot representation of the gas sensor signals for 50 ppm CO, 1000 ppm CH_4, 10 ppm ethanol and 500 ppb toluene in dry air (dashed lines/empty symbols) and 50% r.h. (straight line/filled symbols) of pristine SnO_2 (blue) and Au-loaded SnO_2 (red) at 300 °C. The sensor signals for the material based on SnO_2-1000 are shown in (a), the ones based on SnO_2-450 in (b).

3.1.2. Pd-loaded samples

Compared to the Au-loaded SnO_2 sample, loading SnO_2 with Pd NPs (Fig. 3) has a different effect on the gas response patterns of the sensing materials. In the case of CO, both Pd-loaded materials show low sensor signals in dry air, which are - unlike those of pristine SnO_2 - increased in the presence of humidity. This behavior is well-known for noble metal oxide loaded SMOX. In the case of Pt-loaded SnO_2, it is explained by the interference of H_2O with the surface reduction by CO as well as the re-oxidation by O_2. In dry air neither reduction nor re-oxidation is hindered, and efficient re-oxidation prevents changes in the PtO_x composition, which would cause sensor signals. In humid air water vapor inhibits both reactions, but the inhibiting effect is stronger for the re-oxidation and, thus, the sensor signals increase compared to dry air, while the catalytic activity of the material decreases[26]. A strong difference between the CH_4 gas response of Au/SnO_2 and

Pd/SnO_2 is observed. In dry air Pd/SnO_2 shows strong sensor signals for CH_4, which are decreased by the presence of water vapor, but remain rather high compared to the other sensing materials. Assuming that the activation of the less reactive CH_4 is limiting the methane sensing, a decrease in the CH_4 oxidation activity of PdO under humid conditions would explain the effect of water vapor on the CH_4 signals. And indeed, for PdO-based catalysts used for CH_4 oxidation a reduced activity is found under humid conditions[44]. Differences in ethanol sensing are also observed: Pd/SnO_2-1000 shows a slight increase of the ethanol signals in the presence of water vapor, while Pd/SnO_2-450 shows a slight decrease. These differences may arise from the different surface areas and Pd concentrations in the samples, or in case of ethanol sensing from an interaction with the support. Both Pd-loaded samples show weak response to toluene and are not significantly affected by water vapor.

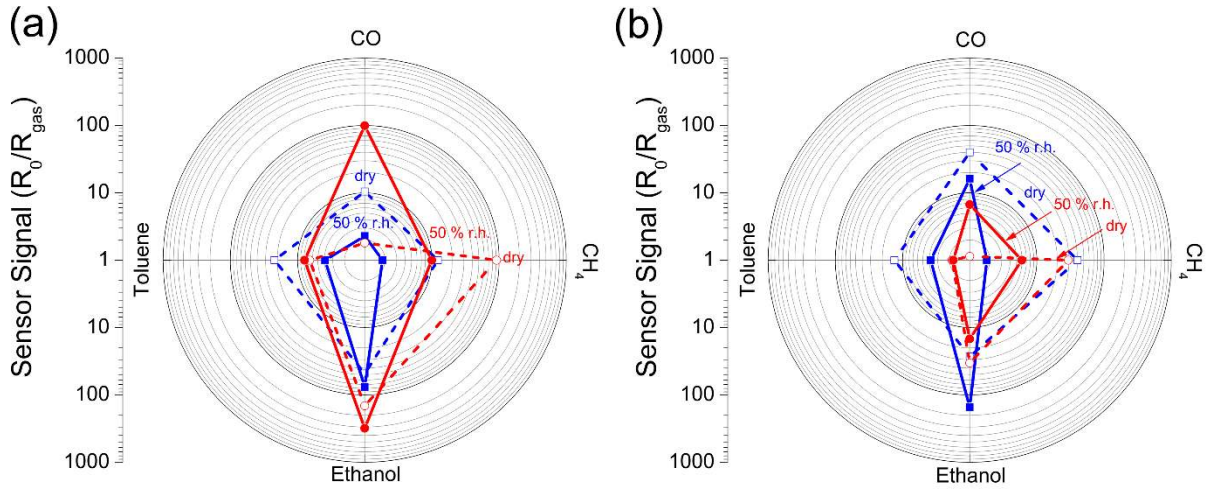

Fig. 3 Polar plot representation of the gas sensor signals for 50 ppm CO, 1000 ppm CH_4, 10 ppm ethanol and 500 ppb toluene in dry air (dashed lines/empty symbols) and 50% r.h. (straight line/filled symbols) of pristine SnO_2 (blue) and Pd-loaded SnO_2 (red) at 300 °C. The sensor signals for the material based on SnO_2-1000 are shown in (a), the ones based on SnO_2-450 in (b).

3.1.3. AuPd-loaded samples

AuPd NPs on SnO_2 (Fig. 4) show once again a different behavior compared to their monometallic systems. Compared to the undoped SnO_2, the AuPd nanoalloy shows lower sensor signals, with a different response pattern to the four gases, and a different susceptibility to water vapor. In the case of both pristine SnO_2 materials, water vapor causes a decrease in the CO signals, while the AuPd/SnO_2 materials provide increased signals. For ethanol the opposite effect compared to the Pd/SnO_2 samples is observed. The AuPd/SnO_2 materials show a strong decrease in the ethanol sensor signals in the presence of water vapor. Unlike Pd/SnO_2, AuPd/SnO_2 samples do not show a pronounced enhancement of the CH_4 sensor signals. The response to toluene remains low. The sensing properties of the AuPd NPs are more similar to those of Pd NPs, but show differences in the selectivity towards CH_4 and the effect of water vapor on the ethanol signals.

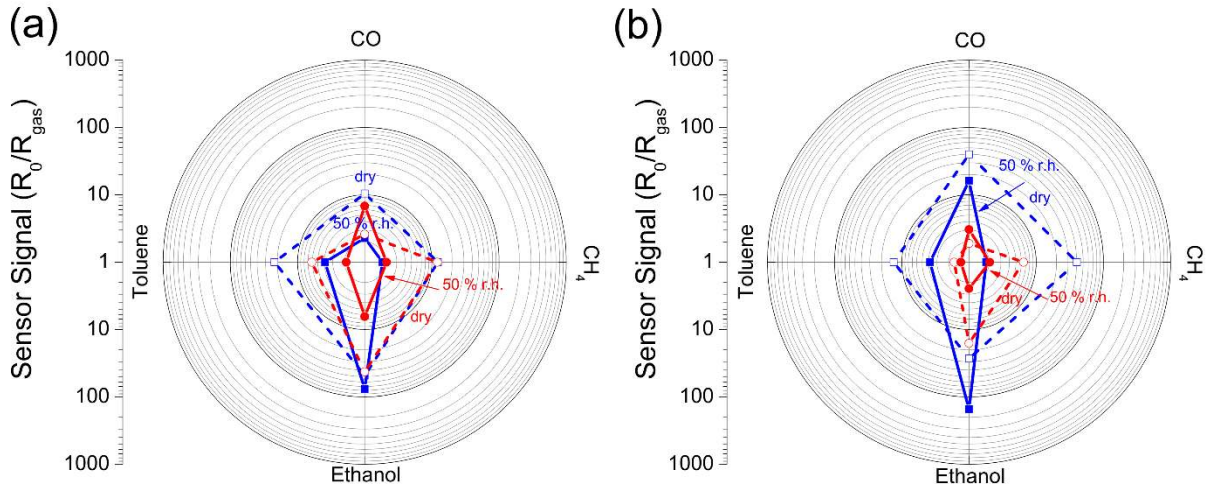

Fig. 4 Polar plot representation of the gas sensor signals for 50 ppm CO, 1000 ppm CH_4, 10 ppm ethanol and 500 ppb toluene in dry air (dashed lines/empty symbols) and 50% r.h. (straight line/filled symbols) of pristine SnO_2 (blue) and AuPd-loaded SnO_2 (red) at 300 °C. The sensor signals for the material based on SnO_2-1000 are shown in (a), the ones based on SnO_2-450 in (b).

On both SnO_2 materials, Pd and AuPd NPs cause response patterns less dependent on the support material, but rather on the noble metal loading. This observation suggests that the gas reception is controlled by the AuPd or Pd NPs, respectively, i.e. the oxidation of the reducible analyte gases dominantly takes place on the noble metal NPs and the charge carrier concentration in SnO_2 is changed due to the electronic coupling of SnO_2 and the noble metal NPs (Fermi-level control). Thus, in the case of a Fermi-level control sensitization, the gas sensing properties, e.g. the selectivity, are defined by the catalytic properties of the noble metal loading, as the gas reception is shifted to the noble metal NPs. In the case of Pd (Fig. 3) and AuPd (Fig. 4) supported on SnO_2, the strong dependency of the sensing properties on the noble metal loadings shows that a Fermi-level controlled sensitization mechanism dominates, i.e. a strong electronic interaction of the noble metal clusters and SnO_2, rather than an activation of the SnO_2 surface, e.g. by a spill-over mechanism as in the case of Au clusters. In case of a spill-over sensitization by gold (Fig. 2), the nature of the support material plays an important role. When comparing the noble metal NPs supported on two differently prepared SnO_2 materials (with two different surface areas) with each other or with their corresponding pristine SnO_2 base materials, differences in the magnitude of the sensor signals maybe explained with differences in the concentration of reactive sites, which depends on noble metal loadings and the surface area of the SnO_2. Despite the strong differences in the magnitude of the sensor signals, it is important to note that all three noble metal loadings cause different response patterns to the test gases, i.e. have a different effect on the selectivity of the gas sensing materials. This is an interesting finding, demonstrating that it is possible to influence the selectivity of gas sensing materials by tuning the composition of the noble metal component.

3.2. Mechanistic investigations

The impact of additives in SMOX gas sensing materials is influenced by various factors; besides their chemical state, i.e. oxide or metal, and structure, their surface concentration has a large impact on the gas sensing properties. Both base materials have different material properties[34-36], but also different grain sizes[33]. In order to achieve a similar surface loading, the absolute loadings were adjusted by a factor similar to the difference in specific surface area. This allows us to discuss the impact of different additives as well as the role of the supporting SMOX properties on the basis of a similar additive surface concentration.

3.2.1. Structural analysis

The morphology and size distributions of the NPs from as prepared gas sensors were analyzed by STEM (Fig. 5 and S3). Size distributions were determined by measuring the diameters of several hundreds of NPs (Fig. S3). Samples with low noble metal loadings on supports with low surface area, i.e. 0.1 wt.% Au(Pd)/SnO_2-1000, exhibited small average diameters (5.8 and 6.6 nm, respectively). Moreover, the alloyed AuPd NPs show a smaller NP size compared to Au NPs. This effect was also reported earlier in our previous work[30] for such monometallic and bimetallic NPs supported on TiO_2; extended-X-ray absorption fine structure (EXAFS) showed that the surface of AuPd NPs after deposition on support material and drying was mostly dominated by segregated Palladium. The presence of both Au and Pd in one single nanoparticle of AuPd nanoalloy is also shown in STEM-EDX spectrum (Fig. S4). Due to low contrast in STEM image between oxidized Pd and the SnO_2 support in the calcined Pd/SnO_2 sample, the Pd NPs could not be clearly detected by electron microscopy (Fig. 5c,f), however the presence of Pd on SnO_2 was confirmed by EDX spectroscopy (Fig. S5 and S6). Previous studies on Pd-loaded SnO_2 gas sensing

materials revealed that Pd is present as PdO on the SnO_2 surface[43, 45] and remains oxidized during sensor operation[43, 46].

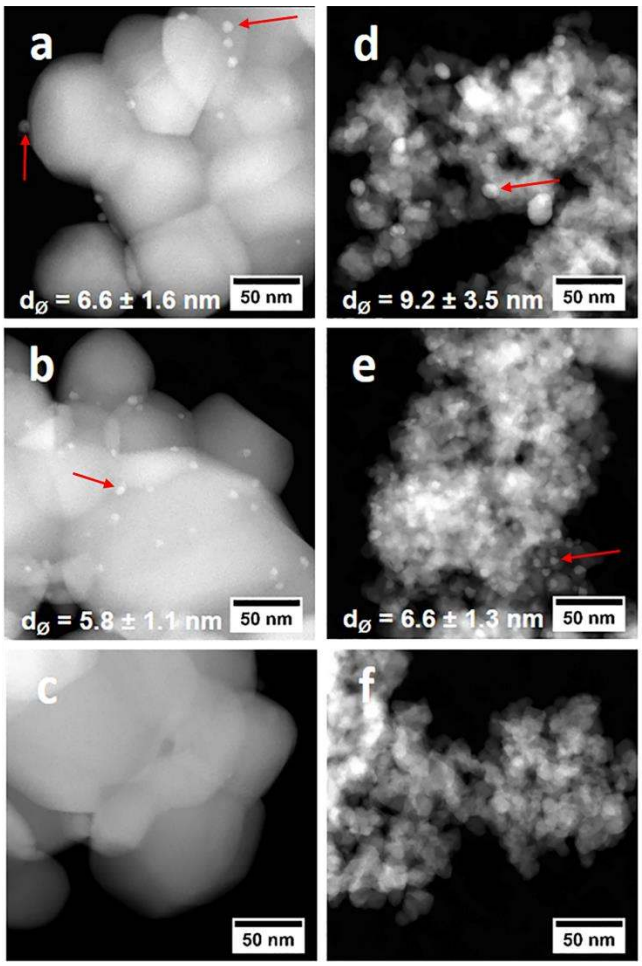

Fig. 5 STEM images of 0.1 wt.% (a) Au, (b) AuPd and (c) Pd supported on SnO_2-1000, and 1.0 wt.% (d) Au, (e) AuPd and (f) Pd supported on SnO_2-450 after gas sensing test at 300 °C. Red arrows indicate representatives of noble metal NPs.

The structural analysis by STEM and the analogy to NPs supported on SnO_2 suggest that for all doped materials the noble metals form clusters on the SnO_2 surface. To further understand the sensitization mechanism, the electrical and chemical impact of the dopants was studied by

estimating the initial surface band bending in an inert atmosphere (pure N_2) and by operando DRIFTS, respectively.

3.2.2. Electronic effects of the loadings

Sensitization by a Fermi-level control mechanism requires an electronic coupling between the noble metal oxide and the supporting SnO_2 support. The electronic coupling will cause an initial band bending independent on adsorbed gases, i.e. also present in an inert atmosphere. Thus, by comparing the resistances of the noble metal loaded materials with the corresponding values for pristine SnO_2 allows estimating the initial band bending using the following equation[26, 47], where eV_S is the initial band bending, k_BT the thermal energy, R_L is the resistance of the noble metal loaded samples in pure N_2, and R_P the resistance of pristine SnO_2 in pure N_2:

$$eV_S = k_BT \cdot ln\left(\frac{R_L}{R_P}\right)$$

The results of these calculations are summarized in Table 1. In addition to the initial band bending and the resistance in nitrogen, the residual oxygen content in the nitrogen atmosphere is shown. The high initial band bending for the samples loaded with Pd or AuPd NPs indicates a strong electronic coupling of SnO_2 and the NPs, while for the samples loaded with Au NPs a lower initial band bending is found. The low initial band bending for Au NPs is comparable with the expected error of this calculation, namely the thermal energy at 300 °C (49 meV), and can be explained by an increased adsorption of residual oxygen related to the expected O_2 spill-over by Au NPs. The calculated initial band bending for the noble metal loaded samples indicates that there is only an electronic coupling for the materials loaded with Pd or AuPd NPs, while in the case of Au NPs there is no strong electronic interaction with the supporting SnO_2 support.

Table 1 Sensor resistances in an inert atmosphere and the calculated initial band bending due to the noble metal dopants. Further details are given in the text.

Sample	Residual O_2 [ppm]	Resistance [Ω]	Band bending [meV]
SnO_2-1000			
undoped	1.7	1224	-
0.1 wt.% Au	1.7	2439	34
0.1 wt.% AuPd	1.7	24007	147
0.1 wt.% Pd	1.7	34100	164
SnO_2-450			
undoped	2.4	145	-
1.0 wt.% Au	2.4	647	74
1.0 wt.% AuPd	2.4	22505	249
1.0 wt.% Pd	2.4	36326	273

3.2.3. Chemical effects of the loadings

Changes in surface chemistry due to loading with noble metal NPs were investigated by operando DRIFTS spectroscopy using CO as reducing gas. On pristine SnO_2, the detection of CO consumes surface oxygen, causing a decrease in the Sn-O overtone vibrations between 1370 and 1330 cm^{-1} on both SnO_2 materials[34]. On SnO_2-1000 additional Sn-O overtone bands are reported at 1271, 1205, 1159 and 1059 cm^{-1}[34]. The decrease in surface oxygen concentration causes a subsequent decrease in surface hydroxyl groups, which are in equilibrium with surface oxygen[34, 42]. The hydroxyl groups show several sharp O-H stretch vibrations between 3750 and 3450 cm^{-1}, one broad band of interacting OH groups (3600 to 2500 cm^{-1}) and the corresponding Sn-OH deformation vibrations (mainly below 1000 cm^{-1})[34]. No adsorbed carbonyls are observed under dry or humid gas sensing conditions (50 ppm CO and 20.5 vol.% O_2). The DRIFTS spectra of all SnO_2-1000 materials during CO sensing are shown in Fig. 6. In dry air (Fig. 6, top), undoped SnO_2 bands related to surface oxygen and hydroxyl groups decrease as described above. In the case of the sample doped with Au NPs, a similar situation occurs. This indicates that gas reception takes

place on the SnO_2 surface, while for the AuPd and Pd NPs loaded samples no changes in the SnO_2 surface are observed. For the latter case, this suggests that the gas reception does no longer take place on the SnO_2 surface, i.e. it is shifted to the AuPd or Pd NPs. In 10% r.h. (Fig. 6, bottom), the strongest change is observed for undoped SnO_2, which shows a lower impact on the SnO_2 surface species due to CO exposure. This correlates with the decreased CO signals in humid air (see Fig. 2-4) and is explained by the previously reported competition of CO and H_2O for the same surface oxygen species[34]. For the samples loaded with Au NPs, humidity does not cause a decrease, i.e. the material remains reactive in the presence of water vapor. This observation explains the low impact of water vapor on the CO sensor signals in humid air (Fig. 2-4). For the samples loaded with AuPd or Pd NPs, one observes a weak increase of surface oxygen and hydroxyl groups on SnO_2. This can be explained by a decreased reactivity of the noble metal NPs in humid air: As recently reported for Pt-loaded SnO_2, water can inhibit re-oxidation of the noble metal clusters and CO oxidation consumes oxygen from the SnO_2 surface[26]. In case of Pt loaded SnO_2, the PtO_x sensitized SnO_2 by a Fermi-level control mechanism and a decreased re-oxidation of the PtO_x clusters during sensing in humid air caused strong changes in the composition of the PtO_x clusters and, thus, a strong effect on the electronic interface of PtO_x and SnO_2, i.e. a stronger change in resistance. The DRIFT spectra of the AuPd and Pd loaded sample suggests that a similar situation as for Pt loaded SnO_2 occurs.

The samples based on SnO_2-450 show the same behavior, i.e. an increased reactivity of the SnO_2 surface for the samples loaded with Au NPs and a decreased interaction of CO with the SnO_2 surface in case of the samples loaded with AuPd or Pd NPs. The decreased interaction of CO with the SnO_2 surface indicates that the gas reception is shifted to the noble metal NPs. However, in dry air an increase in rooted hydroxyl groups (3600 to 3400 cm^{-1}), i.e. OH groups coordinated with

two or three Sn ions[41], on the noble metal samples due to CO exposure is observed. This increase is most likely related to very small changes in the residual humidity in the gas flow due to mixing flows from two different channels and gas bottles.

3.3. Summary

Independent of the base materials, the gas sensing experiments (Fig. 2-4) along with the estimated values for initial band bending (Table 1) and operando DRIFTS results (Fig. 6 and Fig. S7) reveal similar effects for each noble metal loading:

- In case of Au NPs, there is no initial band bending due to the Au loading, i.e. there is no electronic coupling of Au and SnO_2. DRIFTS revealed, that Au enhances the reactivity of the SnO_2 surface. In line with previous works[22, 23], these findings support an oxygen related spill-over sensitization for Au NPs.

- In case of AuPd and Pd NPs a strong initial band bending is found, i.e. there is a strong electronic interaction between SnO_2 and AuPd or Pd, respectively. The DRIFTS spectra of both materials show that the reaction of CO is no longer taking place on the SnO_2 surface and, thus, is shifted to the noble metal clusters. These findings suggest a sensitization by a Fermi-level control mechanism, as recently reported for Pt loaded SnO_2 or Rh loaded WO_3[26, 47].

The similarity between the AuPd and Pd doped sample suggests that a Fermi-level control mechanism determines the sensing properties of the alloy material. The absence of a spill-over sensitization is related to the deactivation of the oxide support by an initial band bending, e.g. as recently reported for Rh loaded WO_3[47]. Thus, it is concluded, that in case of a sensitization by a Fermi-level control mechanism, a spill-over sensitization is absent or does not contribute to the gas reception. In the case of the Fermi-level control sensitization, the sensor signals depend on

changes in the NP composition determined by the interplay of reduction and (re-) oxidation of the catalytically active sites on the NPs under certain conditions[26].

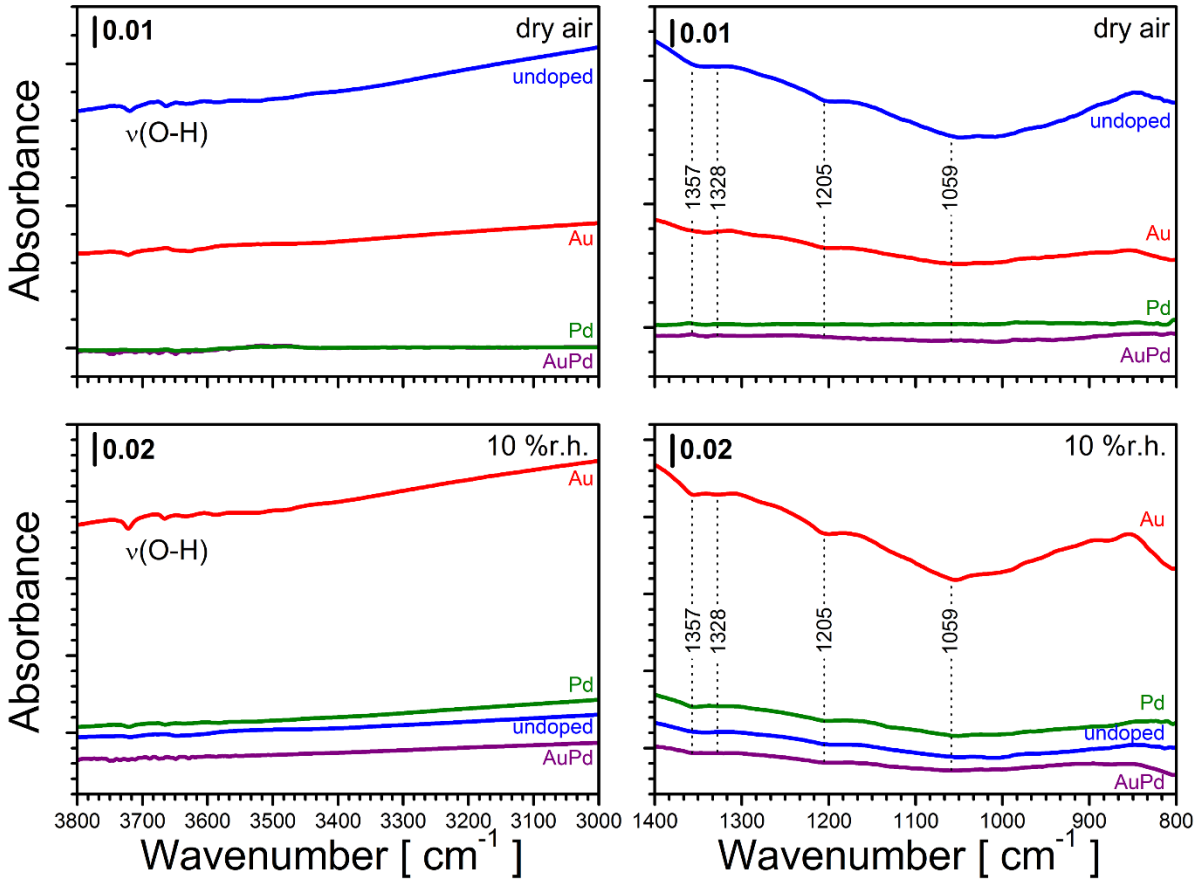

Fig. 6 Operando DRIFT spectra of SnO_2-1000 materials during sensing of 50 ppm CO in dry air (top) and in 10% r.h. (bottom). The spectral regions with the O-H stretch vibrations and the fingerprint region are respectively shown on the left and right side. All sensors were operated at 300 °C.

4. Conclusions and outlook

Colloidal monometallic Au and Pd NPs as well as AuPd nanoalloys were synthesized using a microfluidic reactor with efficient micromixers and then deposited on SnO_2 as support. The gas sensing measurements at 300 °C and especially the comparison of pure Au, AuPd alloy and pure

Pd NPs supported on different SnO_2 substrates demonstrate that the gas sensing properties can be strongly influenced by the noble metal loading and its composition. The investigations on the sensitization mechanism of the materials revealed that for Au oxygen spill-over improves the sensing properties of the SnO_2 surfaces, whereas for the samples with Pd-containing loadings, i.e. AuPd or Pd NPs, a Fermi-level control sensitization mechanism is found to determine the sensing properties of the materials. Moreover, the catalytic reactions over the PdO_x-particles may strongly alter the sensing properties, e.g. for CO. The AuPd nanoalloy differs from the monometallic noble metal loadings and thus, systematically testing further alloy compositions is a promising approach to improve the selectivity of gas sensing materials. In addition to the alloy composition, further optimization of the noble metal concentration, support materials and operation temperature will enhance the potential of this promising type of noble metal NP based sensors.

Supplementary data:

Supplementary data, including additional comparisons of the gas sensing performance, further HAADF-STEM and STEM-EDX analysis of the materials and DRIFT spectra of SnO_2-450, can be found in the online version.

Acknowledgement:

The Virtual Institute VI-403 “In-situ Nano Imaging of Biological and Chemical Processes”, the BMBF (projects 05K10VK1, 05K13VK2), “Science and Technology of Nanosystems” Programme (432202) and KIT are gratefully acknowledged for financial support. Finally, we would like to appreciate the Karlsruhe Nano Micro Facility (KNMF), a Helmholtz research infrastructure at KIT, for providing STEM-EDX measurements.

References:

[1] N. Bârsan, G. Gauglitz, A. Oprea, E. Ostertag, G. Proll, K. Rebner, K. Schierbaum, F. Schleifenbaum, U. Weimar, Chemical and biochemical sensors, 1. Fundamentals. Ullmann's Encyclopedia of Industrial Chemistry, 2012.
[2] S.A. Müller, D. Degler, C. Feldmann, M. Türk, R. Moos, K. Fink, F. Studt, D. Gerthsen, N. Bârsan, J.-D. Grunwaldt, Exploiting synergies in catalysis and gas sensing using noble metal-loaded oxide composites, ChemCatChem 10 (2018) 864-880.
[3] D. Briand, J. Courbat, Micromachined semiconductor gas sensors, in: R. Jaaniso, K. Tan (Eds.), Semiconductor Gas Sensors, Elsevier, 2013, pp. 220-260.
[4] J. Spannhake, A. Helwig, O. Schulz, G. Müller, Micro-fabrication of gas sensors, Solid State Gas Sensing, Springer, 2009, pp. 1-46.
[5] K. Ihokura, J. Watson, The Stannic Oxide Gas Sensor Principles and Applications, CRC press, 1994.
[6] G.D. Chansin, Printed and Flexible Sensors 2015-2025: Technologies, Players, Forecasts, IDTechEx Limited, 2015.
[7] D. Kohl, Surface processes in the detection of reducing gases with SnO_2-based devices, Sens. Actuators 18 (1989) 71-113.
[8] T. Sahm, W. Rong, N. Bârsan, L. Mädler, U. Weimar, Sensing of CH_4, CO and ethanol with in situ nanoparticle aerosol-fabricated multilayer sensors, Sens. Actuators, B: Chem. 127 (2007) 63-68.
[9] N. Bârsan, U. Weimar, Conduction model of metal oxide gas sensors, J. Electroceramic. 7 (2001) 143-167.
[10] R. Jaaniso, O.K. Tan, Semiconductor Gas Sensors, Elsevier, 2013.
[11] H.W. Carvalho, D. Degler, N. Bârsan, J.-D. Grunwaldt, in: Y. Iwasawa, K. Asakura, M. Tada (Eds.), XAFS Techniques for Catalysts, Nanomaterials, and Surfaces, Springer, 2017, pp 383-396.
[12] D. Kohl, The role of noble metals in the chemistry of solid-state gas sensors, Sens. Actuators, B: Chem. 1 (1990) 158-165.
[13] A. Cabot, J. Arbiol, J.R. Morante, U. Weimar, N. Bârsan, W. Göpel, Analysis of the noble metal catalytic additives introduced by impregnation of as obtained SnO_2 sol–gel nanocrystals for gas sensors, Sens. Actuators, B: Chem. 70 (2000) 87-100.
[14] N. Ma, K. Suematsu, M. Yuasa, T. Kida, K. Shimanoe, Effect of water vapor on Pd-loaded SnO_2 nanoparticles gas sensor, ACS Appl. Mater. Interfaces 7 (2015) 5863-5869.
[15] H.-J. Kim, J.-H. Lee, Highly sensitive and selective gas sensors using p-type oxide semiconductors: Overview, Sens. Actuators, B: Chem. 192 (2014) 607-627.
[16] A. Cabot, A. Diéguez, A. Romano-Rodríguez, J. Morante, N. Bârsan, Influence of the catalytic introduction procedure on the nano-SnO_2 gas sensor performances: Where and how stay the catalytic atoms?, Sens. Actuators, B: Chem. 79 (2001) 98-106.
[17] M. Hübner, N. Bârsan, U. Weimar, Influences of Al, Pd and Pt additives on the conduction mechanism as well as the surface and bulk properties of SnO_2 based polycrystalline thick film gas sensors, Sens. Actuators, B: Chem. 171-172 (2012) 172-180.
[18] J. Rebholz, P. Bonanati, C. Jaeschke, M. Hübner, L. Mädler, U. Weimar, N. Bârsan, Conduction mechanism in undoped and antimony doped SnO_2 based FSP gas sensors, Sens. Actuators, B: Chem. 188 (2013) 631-636.
[19] D. Degler, H.W.P. de Carvalho, K. Kvashnina, J.-D. Grunwaldt, U. Weimar, N. Bârsan, Structure and chemistry of surface-doped Pt: SnO_2 gas sensing materials, RSC Adv. 6 (2016) 28149-28155.
[20] K. Großmann, S. Wicker, U. Weimar, N. Bârsan, Impact of Pt additives on the surface reactions between SnO_2, water vapour, CO and H_2; an operando investigation, Phys. Chem. Chem. Phys. 15 (2013) 19151-19158.
[21] G. Korotcenkov, V. Brinzari, L. Gulina, B. Cho, The influence of gold nanoparticles on the conductivity response of SnO_2-based thin film gas sensors, Appl. Surf. Sci. 353 (2015) 793-803.

[22] M. Hübner, D. Koziej, J.-D. Grunwaldt, U. Weimar, N. Bârsan, An Au clusters related spill-over sensitization mechanism in SnO_2-based gas sensors identified by operando HERFD-XAS, work function changes, DC resistance and catalytic conversion studies, Phys. Chem. Chem. Phys. 14 (2012) 13249-13254.
[23] D. Degler, S. Rank, S. Mueller, H.W. Pereira de Carvalho, J.-D. Grunwaldt, U. Weimar, N. Bârsan, Gold-loaded tin dioxide gas sensing materials: Mechanistic insights and the role of gold dispersion, ACS Sens. 1 (2016) 1322-1329.
[24] C. Liu, Q. Kuang, Z. Xie, L. Zheng, The effect of noble metal (Au, Pd and Pt) nanoparticles on the gas sensing performance of SnO_2-based sensors: A case study on the {221} high-index faceted SnO_2 octahedra, CrystEngComm. 17 (2015) 6308-13.
[25] Y. Sakai, M. Kadosaki, I. Matsubara, T. Itoh, Preparation of total VOC sensor with sensor-response stability for humidity by noble metal addition to SnO_2, J. Ceram. Soc. Jpn. 117 (2009) 1297-1301.
[26] D. Degler, S.A. Müller, D.E. Doronkin, D. Wang, J.-D. Grunwaldt, U. Weimar, N. Bârsan, Platinum loaded tin dioxide: A model system for unravelling the interplay between heterogeneous catalysis and gas sensing, J. Mater. Chem. A 6 (2018) 2034-2046.
[27] N. Yamazoe, New approaches for improving semiconductor gas sensors, Sens. Actuators, B: Chem. 5 (1991) 7-19.
[28] S. Matsushima, Y. Teraoka, N. Miura, N. Yamazoe, Electronic interaction between metal additives and tin dioxide in tin dioxide-based gas sensors, Jpn. J. Appl. Phys. 27 (1988) 1798.
[29] M. Hübner, A. Sackmann, F. Gyger, C. Feldmann, P. Bockstaller, D. Gerthsen, U. Weimar, N. Bârsan, Location effect of Pd additives on the detection of reducing gases for nanoscale SnO_2 hollow spheres based gas sensors, Procedia Eng. 47 (2012) 208-211.
[30] G. Tofighi, A. Gaur, D.E. Doronkin, H. Lichtenberg, W. Wang, D. Wang, G. Rinke, A. Ewinger, R. Dittmeyer, J.-D. Grunwaldt, Microfluidic synthesis of ultrasmall AuPd nanoparticles with a homogeneously mixed alloy structure in fast continuous flow for catalytic applications, J. Phys. Chem. C 122 (2018) 1721-1731.
[31] G. Tofighi, H. Lichtenberg, J. Pesek, T.L. Sheppard, W. Wang, L. Schöttner, G. Rinke, R. Dittmeyer, J.-D. Grunwaldt, Continuous microfluidic synthesis of colloidal ultrasmall gold nanoparticles: In situ study of the early reaction stages and application for catalysis, React. Chem. Eng. 2 (2017) 876-884.
[32] N. Hayashi, Y. Sakai, H. Tsunoyama, A. Nakajima, Development of ultrafine multichannel microfluidic mixer for synthesis of bimetallic nanoclusters: Catalytic application of highly monodisperse AuPd nanoclusters stabilized by poly (N-vinylpyrrolidone), Langmuir 30 (2014) 10539-10547.
[33] A. Diéguez, A. Romano-Rodríguez, J.R. Morante, J. Kappler, N. Bârsan, W. Göpel, Nanoparticle engineering for gas sensor optimisation: improved sol–gel fabricated nanocrystalline SnO_2 thick film gas sensor for NO_2 detection by calcination, catalytic metal introduction and grinding treatments, Sens. Actuators, B: Chem. 60 (1999) 125-137.
[34] D. Degler, S. Wicker, U. Weimar, N. Bârsan, Identifying the active oxygen species in SnO_2 based gas sensing materials: An operando IR spectrsocopy study, J. Phys. Chem. C 119 (2015) 11792-11799.
[35] S. Wicker, M. Guiltat, U. Weimar, A. Hémeryck, N. Barsan, Ambient humidity influence on CO detection with SnO_2 gas sensing materials. A combined DRIFTS/DFT investigation, J. Phys. Chem. C 121 (2017) 25064-25073.
[36] D. Degler, N. Barz, U. Dettinger, H. Peisert, T. Chassé, U. Weimar, N. Barsan, Extending the toolbox for gas sensor research: Operando UV/vis diffuse reflectance spectroscopy on SnO_2-based gas sensors, Sens. Actuators, B: Chem. 224 (2016) 256-259.
[37] N. Bârsan, M. Hübner, U. Weimar, Conduction mechanisms in SnO_2 based polycrystalline thick film gas sensors exposed to CO and H_2 in different oxygen backgrounds, Sens. Actuators, B: Chem. 157 (2011) 510-517.
[38] J. Rebholz, C. Dee, U. Weimar, N. Barsan, A self-doping surface effect and its influence on the sensor performance of undoped SnO_2 based gas sensors, Procedia Engineer. 120 (2015) 83-87.
[39] N. Bârsan, U. Weimar, Understanding the fundamental principles of metal oxide based gas sensors; the example of CO sensing with SnO_2 sensors in the presence of humidity, J. Phys.: Condens. Matter 15 (2003) R813.

[40] C.A. Schneider, W.S. Rasband, K.W. Eliceiri, NIH Image to ImageJ: 25 years of image analysis, Nat. Methods 9 (2012) 671-675.
[41] S. Harbeck, A. Szatvanyi, N. Bârsan, U. Weimar, V. Hoffmann, DRIFT studies of thick film un-doped and Pd-doped SnO_2 sensors: Temperature changes effect and CO detection mechanism in the presence of water vapour, Thin Solid Films 436 (2003) 76-83.
[42] K. Grossmann, R.G. Pavelko, N. Bârsan, U. Weimar, Interplay of H_2, water vapor and oxygenat the surface of SnO_2 based gas sensors–An operando investigation utilizing deuterated gases, Sens. Actuators, B: Chem. 166 (2012) 787-793.
[43] D. Degler, H.W.P. de Carvalho, U. Weimar, N. Bârsan, D. Pham, L. Maedler, J.-D. Grunwaldt, Structure–function relationships of conventionally and flame made Pd-doped sensors studied by X-ray absorption spectroscopy and DC-resistance, Sens. Actuators, B: Chem. 219 (2015) 315-323.
[44] A.T. Gremminger, H.W.P. de Carvalho, R. Popescu, J.-D. Grunwaldt, O. Deutschmann, Influence of gas composition on activity and durability of bimetallic Pd-Pt/Al_2O_3 catalysts for total oxidation of methane, Catal. Today 258 (2015) 470-480.
[45] A.V. Marikutsa, M.N. Rumyantseva, D.D. Frolov, I.V. Morozov, A.I. Boltalin, A.A. Fedorova, I.A. Petukhov, L.V. Yashina, E.A. Konstantinova, E.M. Sadovskaya, Role of PdO_x and RuO_y clusters in oxygen exchange between nanocrystalline tin dioxide and the gas phase, J. Phys. Chem. C 117 (2013) 23858-23867.
[46] D. Koziej, M. Hübner, N. Bârsan, U. Weimar, M. Sikora, J.-D. Grunwaldt, Operando X-ray absorption spectroscopy studies on Pd-SnO_2 based sensors, Phys. Chem. Chem. Phys. 11 (2009) 8620-8625.
[47] A. Staerz, T.-H. Kim, J.-H. Lee, U. Weimar, N. Bârsan, Nanolevel control of gas sensing characteristics via p–n heterojunction between Rh_2O_3 clusters and WO_3 crystallites, J. Phys. Chem. C 121 (2017) 24701-24706.

Graphical abstract: